2019

High-throughput Prediction and Stabilization of Electride-Halide Material Systems

Jack Sundberg

Principle Investigator: Dr. Scott Warren
Oral Defense: April 18th, 2019; 3:00pm Caudill 221

Department of Chemistry, Polymer/Materials Division
The University of North Carolina – Chapel Hill

CONTENTS:

1. Introduction to Electride-Halide Analog Pairs

Electrides have gained considerable attention in recent literature thanks to applications as superconductors, co-catalysts, and solid-state dopants. To this end, a single electride material (Ca_2N) has demonstrated conductivities competitive with silver[1], catalytic activity for ammonia production at low temperature[2], and sufficient electron doping to induce a phase change in $MoTe_2$(3). This advanced performance derives from an electride's defining property: bare-electrons that exist at isolated lattice sites. Thus, the lone electrons are often referred to as anionic electrons, making a compound like Ca_2N more accurately represented with a formula $[Ca_2N]^+ \cdot e^-$ (where oxidation states of Ca and N are 2+ and 3-, respectively).

This atypical motif is more easily understood by comparison of an electride to its halogenated analog. For example, $[Ca_2N]^+ \cdot e^-$ possesses the chloride analog Ca_2NCl, and in this electride-halide analog pair (EHAP), the structures can be viewed as substitution derivatives of e^- for Cl^- and vice-versa. Here, the EHAP is that of a chloride analog, whereas the full electride-halide material system (EHMS) is defined by all halide analogs for a given electride (e.g. Ca_2N with Ca_2NX; X = F, Cl, Br, I) (Figure 1). Previously in literature, an EHAP has strictly been used to aid in describing an electride; however in this prospectus, the idea of an EHMS is introduced and developed towards (i) synthesizing novel electrides and (ii) producing halide-ion batteries.

The synthesis of electride materials has been exclusively carried out via high-temperature, stoichiometric reactions.[4] This limits experimentally known electrides to well-behaved systems in which the target electride is the thermodynamically favored phase. Even in these cases, the majority of electrides represent extremely challenging syntheses due to competing phases. Inspection of the EHMS suggests an alternative synthetic approach: low-temperature dehalogenation of the electride's halide analog. Whether this is done via electrochemical or alkali-vapor etching, the low temperature synthesis permits selection against competing phases via kinetic trapping. Further, proposing synthesis via electrochemical etching raises the plausibility of developing halide-ion batteries. This is because the EHAP could act as a halide-ion electrode should the (de)halogenation be reversible. Together, both applications highlight the promise of investigating EHMS's, whether the end goal be electride synthesis or novel fluoride-ion batteries.

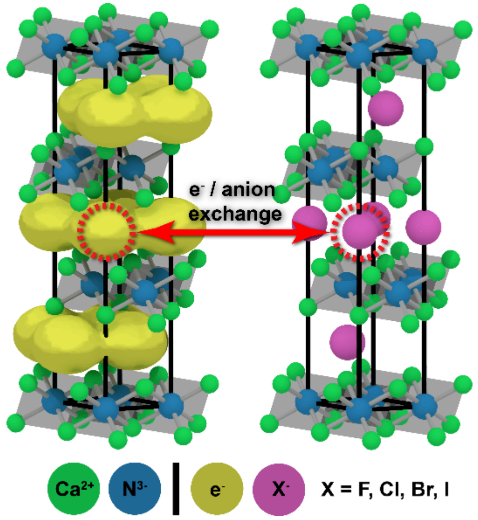

Figure 1. An example electride $[Ca_2N]^+ \cdot e^-$ (left) with an arbitrary halide analog (right). The pair represents an EHAP as they are isostructural – only differing by substitution of e^- for X^-. All anion derivatives (e^-, F^-, Cl^-, Br^-, I^-) together make up the EHMS.

With these two applications in mind, we aim to synthesize previously inaccessible electrides as well as identify new EHMS's for the same. A conventionally used phase-preference strategy – namely, substrate epitaxy – is applied in coordination with an EHMS perspective. Heavily guided by density functional theory (DFT) calculations, an automated workflow will identify the optimal synthetic strategy for a given electride/halide material and allow rapid analysis of other systems. The synthetic approach is first demonstrated with previously reported electrides, while a concurrent systematic search identifies novel EHMS's. The screening for new systems is driven by known halide materials, where the halides are determined to have low diffusion barriers as predicted by DFT. Together, viewing electrides from an EHAP perspective will realize previously inaccessible electrides and extend electride applications toward halide-ion batteries.

2. Synthesis of Electride Materials

Here we outline a generalizable synthetic strategy for 1-, 2-, and 3-dimensional (D) electrides, where the dimensionality refers to the connectivity of anionic electron sites (see Figure 2 for clarification). This excludes discussion of pressure-induced electrides (e.g. Na-metal) and much more stable 0-D "caged" electrides (e.g. $Ca_{24}Al_{28}O_{64}$). Previously, successful syntheses have been reported but are largely inconsistent in practice due to two key obstacles: phase selectivity and vulnerability to oxidation. Thus, synthesis of 1,2,3-D electrides is deemed extremely challenging and in need of an improved approach. Undesirable oxidation is negated via building a custom vacuum system and illustrated with benchmark bulk synthesis (section 2a). Phase selectivity is addressed via a thin-film synthesis rather

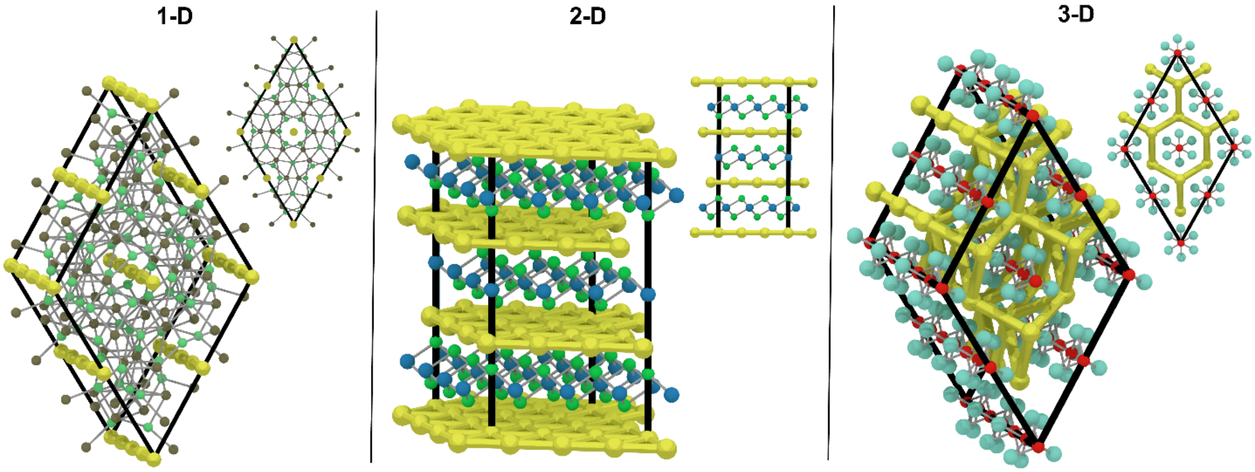

Figure 2. The dimensionality of an electride network is based on the connectivity of the anionic electron lattice positions. Shown are superlattices of the 1-D electride La_5Pb_3 (left), 2-D electride Ca_2N (middle), and 3-D electride Cs_3O (right) where the electride network is in yellow. Insets are alternative perspectives of the superlattice. It is important to note that Cs_3O is likely not a 3-D electride in reality, as each anionic electron site is largely isolated (>6 Å separation) and e^- exchange between positions would be extremely rare. We still show it as such to serve as an example because no 3-D electrides have been reported.

than bulk, as a thin-film synthesis allows for phase stabilization through analysis of film-substrate interactions in addition to an EHMS-perspective strategy (section 2b).

2.a. Bulk Synthesis and Material Instability

Because oxidation can be so prominent in electride syntheses, it is useful to look at a bulk synthesis where electride decomposition can be more accurately quantified. We select Sr_2N (isostructural to Ca_2N) as a benchmark for the reason that attempted syntheses of this 2-D electride often result in significant oxidation relative to other electrides.

We found that oxidation-free product was consistently attained only via intensive oxidation-deterring procedures. Pre-baking of the reaction vessel components (quartz tube, stainless steel inner tube, and molybdenum foil) is done at 350°C for 5 hrs while under 25sccm Ar flow at 130 mTorr. A gas-purifier (NuPure Eliminator®) was added to reduce H_2O, O_2, CO, CO_2, and H_2 impurities to <1 ppb levels. Sr_2N was then synthesized by direct reaction of strontium metal (99.99%, Sigma) with nitrogen (99.999%, Airgas) at 750°C for 12 hours while under 100sccm N_2 flow at 770 Torr.[5] Annealing of the product is carried out at 500°C for 12 hours while under 25sccm Ar at 50 Torr, yielding a black solid. This was all accomplished by performing component assembly in an Ar-filled glovebox (<10 ppb O_2) and using a custom vacuum system (Figure 3a).

The crystal structure is confirmed via X-ray powder diffraction (XRD) as compared to the calculated spectrum (Figure 3b). Identical lattice spacings of the product to those in the literature indicate phase-pure, oxidation-free Sr_2N was successfully synthesized. The high-quality synthesis of our benchmark suggests that the oxidation-deterring procedures are robust enough for thin-film syntheses of equal or less oxidation-prone materials. With Sr_2N being among the most oxidation-sensitive electrides, the demonstrated ability to synthesize Sr_2N illustrates the level of synthetic control attained in the custom reactor.

2.b. Thin-film Synthesis via Substrate Stabilization

Bulk syntheses are largely limited in the choice of phases that can be synthesized, where temperature, pressure, and reactant stoichiometry are the typical parameters used to control thermodynamically stable phases. All three of these are possible with the vacuum system used above, but we aim to synthesize materials that possess significant phase competition and/or exist as a metastable state themselves. The two most common solutions are to attempt phase selectivity by kinetic trapping and by film-substrate interactions. Here, we seek to employ a combined approach with these strategies. A successful synthesis would represent the first kinetic trapping approach as well as the first thin-films of 1,2,3-D electrides. (Note: a strictly kinetic-trapping/EHMS-perspective strategy for bulk electrides is ongoing by other students in the lab – it is therefore not included in this discussion)

The phase-stability of a given electride/halide thin film (E_{thinfilm}) will largely depend on a several contributions, where the relative energy versus hull of a bulk phase (E_{bulk}) is adjusted by:

$$E_{thinfilm} = E_{bulk} + (E_D + E_S + E_E + E_{CT})$$

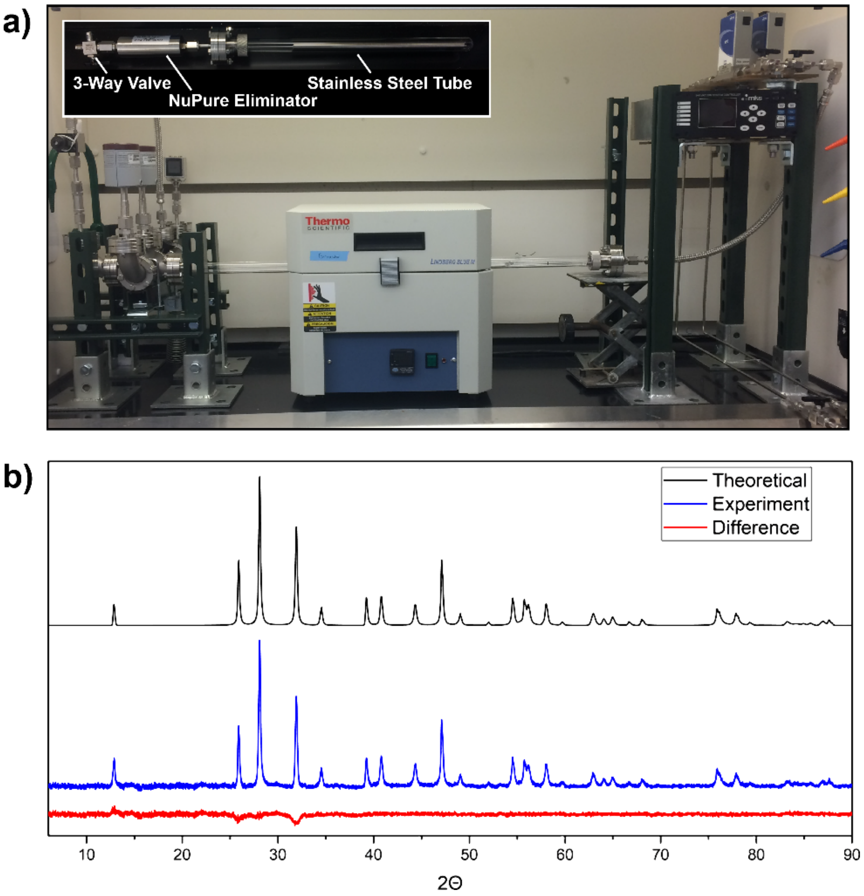

Figure 3. (a) The custom vacuum system built for this project. The main image is a standard chemical vapor deposition assembly, where gas flow is put through a quartz tube and furnace; however, extremely oxidation-sensitive syntheses require a reaction chamber that can be isolated for system purging and transfer between the glovebox and setup. A stainless steel tube is also needed to prevent oxygen-species formation from quartz etching. The reaction chamber meeting these requirements is shown in the inset image. **(b)** XRD pattern of bulk Sr_2N synthesized using the reactor system shown in (a). Pattern is compared to that of calculated (theoretical) shifts from the ICSD database[6]. Data was acquired using the Rigaku Smartlab diffractometer.

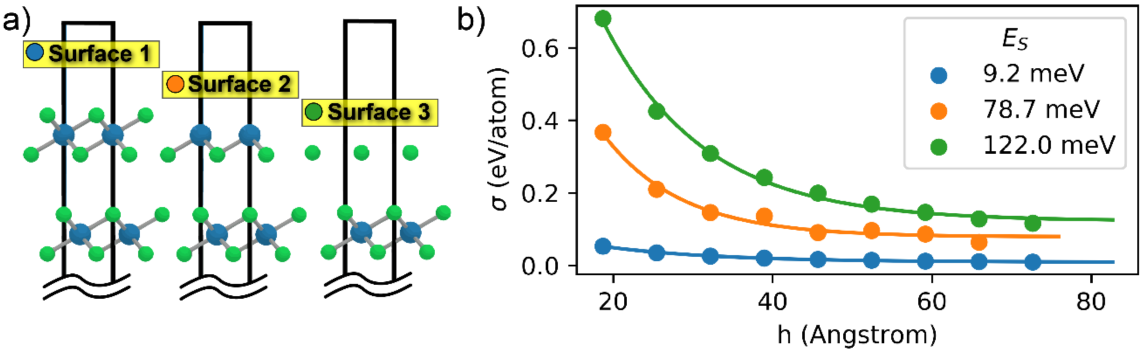

Figure 4. (a) The three slabs generated from the unique 111 surfaces of Ca_2N. Note that the miller index is described with primitive cell basis vectors – see inset of Figure 5b for visualization. The colored circles next to each label refer to the respective data in (b). **(b)** Surface energy calculations for each surface shown in (a). Variables σ and h refer to $\sigma = E_S + E_D$ and slab thickness (not including vacuum space), as defined in the main text. The inset legend refers to calculated surface energies attained by a best fit of the data to an exponential decay.

where E_D, E_S, E_E, and E_{CT} correspond to the energies of dimensionality, surface, elastic, and charge-transfer, respectively. While the lattermost factor has a stabilization effect, the remaining destabilize a given film. We will discuss these factors using an example EHAP (Ca_2N-Ca_2NCl), where the full analysis is automated via use of a data-mining package (PyMatGen)[7] and therefore easily extended to other systems.

2.b.i. Film Orientation and Thickness

The impact of dimensionality is largely sensitive to the specific orientation of the film as well as the atomic terminations of its surface/interface. Therefore, all possible orientations and terminations must be isolated. Symmetrically distinct miller indices are attained via analysis the structure's reciprocal lattice up to a maximum miller index, and all possible unique surface terminations are then isolated using a threshold of 0.1 Å to determine if atoms are on the same plane. A series of 10 slabs are then generated for each miller index and each of its surface terminations, where each slab in the series is an increment thickness of the hkl d-spacings. Slabs were made with 15 Å vacuum spacing and tested for inversion symmetry to ensure both sides of the slab had identical terminations. All unrelaxed slab energies were calculated and compared to that of the bulk, where the energy σ is defined as $\sigma = \frac{1}{2}\left(\frac{E_{slab}}{N_{slab}} - \frac{E_{bulk}}{N_{bulk}}\right)$, with energies ($E$) and number of atoms ($N$) of the slab and bulk unitcell structures, respectively. The energy σ is a combination of the surface energy as well as the dimensional confinement of the slab ($\sigma = E_D + E_S$). Therefore, $\sigma = E_S$ when thickness $= \infty$. Fitting of these slab calculations to an exponential decomposes σ to its components E_D and E_S (see Section 5 for calculation details).

The (111) surface and possible terminations for Ca_2N and Ca_2NCl are shown in Figure 4a, and their corresponding E_S fits in Figure 4b. Results for the other unique surfaces are summarized in Table 1, which only report the lowest energy termination for each miller index. These data are critical for analysis of the latter two components for phase-stability. On its own, we can see particular surfaces are heavily favored, such as the (111) face of Ca_2N. This indicates that there will be strong preferential orientation in film growth, and a more rigorous means of phase-stabilization is needed if a (100) orientation film is desired (e.g. for improved halide-ion battery kinetics). Further, the slab series for (100) orientation film suggest that synthesis of a film below 10 nm is near impossible due to exponentially increasing metastability of the (100) orientation relative to the (111) as thickness approaches a monolayer.

Table 1. Calculated surface energies for Ca_2N

Miller Index	*minimum E_S (meV)*
100	36.1
110	46.1
10-1	80.2
111	9.2

2.b.ii. Topological Elastic Energy

Epitaxial analysis for the substrate-film systems is carried out using a heterostructural topology-matching algorithm.[8] Through iterative reduction of superlattice basis vectors and application of integer-area transformation matrices[9], the methodology identifies the minimal coincident interfacial area (MCIA) for given surface vectors of a substrate and film. Cutoff criteria limits output matches to those with an MCIA less than 400 Å^2 and 9% strain of film. The strain energy E_E associated with film-to-superlattice match is found using the DFT-calculated elastic tensor[10].

The Materials Project[11] employs this algorithm to a pool of 81 substrates and all unique film-substrate miller index combinations. This is intended to recommend an ideal substrate for film synthesis; however, the substrate analysis has two critical flaws that make online-reported results impractical: no analysis is carried out for chemical compatibility of substrates with the film; and matching of all film (and even substrate) miller indices may include those that are unstable. In the case of Ca_2N, it is instantly clear that substrates such as SiO_2 should not be included – Ca will etch SiO_2 to form CaO, as predicted by the Ellingham Diagrams of the two systems and as verified in practice.[12] Further, high energy faces such as the Ca_2N (10-1) should be excluded from analysis for being highly unstable (see Table 1). This leads to a significant amount of data that is misleading and difficult to propose a synthesis from.

While our orientation/dimensionality analysis addresses the latter issue, there is unfortunately no way to thoroughly analyze film-substrate chemical compatibility. Ideally, Ellingham diagrams would be constructed for all material types (oxides, nitrides, carbides, ...) and based on the expected reaction temperature, etchable substrates would be removed. We instead adopt a much more rapid approach to avoid intensive finite-temperature calculations. Interfacial reactions can be predicted via examination of reaction energies as a function of variable mixing.[13] That is, a hull diagram can be made using the film-substrate compounds and all known materials in the Material Project Database. For example, the potential reactions of Ca_2N and SiO_2 (the reactants) can be predicted by searching for known materials (the products) that satisfy conservation of mass and negative formation energy for a given mixing x in $[x \cdot Ca_2N + (1-x) \cdot SiO_2]$ (Figure 5a). With this methodology employed, we can rapidly automate removal of chemically incompatible substrates without any personal calculations. Together, removal of unstable surfaces and substrates allows for an accurate representation of substrate epitaxy. Without further workup, we can see that the (001)-AlN is the ideal substrate for a film of (001)-Ca_2N (Figure 5b).

2.b.iii. Charge Transfer

Thus far, we have extensively characterized the phase stability of a thin-film relative to dimensionality, surface energy, and elastic energy. The final component for an individual material is that of charge-transfer, E_{CT}. In most cases, this energy is negligible, but we found significant bonding character across interfaces with 2-D electrides relative to

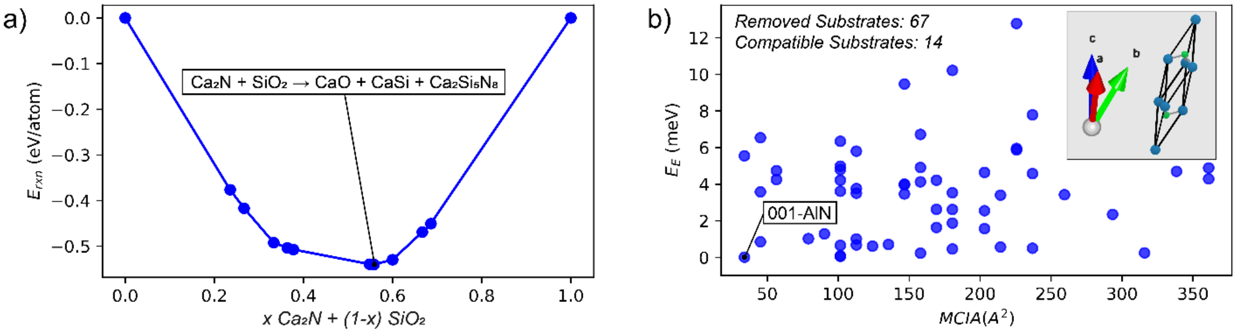

Figure 5. (a) an example convex hull used to analyze potential reactions between Ca_2N and SiO_2 as a function of molar ratio. In a closed system at 0 K, the most favorable products are CaO, CaSi, and $Ca_2Si_5N_8$ with an E_{rxn} of -540 meV. Adding a prediction basis for entropic factors such as temperature, gas partial pressures, and product disorder is ongoing, where we aim to more accurately predict reactions in a semi-open system at expected reaction temperature. **(b)** the result of Ca_2N epitaxial analysis after removal of chemically incompatible substrates and limitation to the 111 orientation of Ca_2N. Of the 81 substrates (see 'Crystal Substrates' on MTI Corp's website[14]), only 14 substrate materials were found to have an E_{rxn} below -100 meV – where the E_{rxn} for each substrate is defined as the minimum hull energy of the Ca_2N-[substrate] analysis shown in (a). The overall best match (001-AlN) is labeled, where AlN reaction analysis had an E_{rxn} of -8 meV. The inset shows the Ca_2N primitive cell that was used for epitaxial matching.

standard films.[15] The massively electron-donating character of electrides toward a substrate could provide added stabilization of the structure, and therefore, should be investigated.

Analogous to our prior studies, the calculations for charge transfer are straightforward. A heterostructure should be formed and used to determine interlayer interaction energies, electron density differences, and doping levels. Going through this process as done previously would be highly inefficient and, in many cases, impossible to do. Formerly, only layered structures were analyzed via topological matching of (001) faces with already matching angle (γ) between a and b lattice vectors. The superlattice match was also determined via $nxnx1$ superlattice steps. The topological matching employed in Section 2.b.ii represents a far superior method. Any miller index combination can be matched, and the reduction of basis vectors allows for $nxmx1$ where n and m need not necessarily be integers. This allows for the smallest possible MCIA and consequently less-taxing calculations. The analysis in Section 2.b.i. also determines the optimal surface termination and thickness for a given orientation. The process can thus be automated for rapid heterostructure formation and analysis of charge transfer.

One obstacle remains for heterostructure formation. In the epitaxy analysis, only surface vector matching is analyzed, whereas a full heterostructure requires c vectors to be parallel. Only then can the film and substrate slabs be imposed in a common unitcell. This problem is simplified if we attempt to force the c vector to be orthogonal to the topologically matched surface. PyMatGen attempts this via a Lenstra–Lenstra–Lovász (LLL) lattice basis reduction algorithm[16]. The algorithm solves for a nearly orthogonal basis vectors, where angles $\alpha=\beta=\gamma=90°$ are not always achieved due to symmetry restrictions of the structure and the a,b-surface epitaxial match is lost. Instead, periodicity of the structure can be maintained by leaving the a, b, and γ surface components while forcing the c-vector to be exactly orthogonal to the surface. By example, the AlN-Ca_2N substrate-film pair is easily formed and used for charge transfer analysis.

2.c. Future Work

The synthetic framework has been laid out and benchmarked both experimentally and computationally. As-is, the custom vacuum system and python libraries maximize chance of successfully synthesizing an oxidation-free (111)-Ca_2N thin film on chemically compatible, epitaxially matched (001)-AlN. While this synthesis will be carried out promptly, the methodology can be extended to more sensitive EHMS's. The efficient comparison of competing phases should be explored next. Extension of principles outlined in Section 2.b. can be used to maximize stabilization effects for the desired phase, while minimizing those for competing phases. This approach has resulted in the syntheses of metastable phases < 75 meV/atom above hull when solely using epitaxy[8], and should charge-transfer be exploited as well, I expect that phases >150 meV/atom above hull will become experimentally accessible. When targeting a specific EHMS, one needs only to identify the lowest $E_{thinfilm}$ for a desired phase relative to the competing phases – then access the EHAP via kinetically-trapped (de)halogenation.

For example, Ca_2N has a +61 meV formation energy relative to Ca_3N_2, which is favored in an open system.[17] The synthesis of a Ca_2N thin-film would be limited to a physical vapor deposition synthesis, rather than a chemical vapor deposition with Ca-metal and N_2 flow. Two options exist to counteract this challenge: first, selecting a substrate that produces a >61 meV stabilization effect for Ca_2N relative to Ca_3N_2; or second, proposing a synthesis for a Ca_2NX halide analog, which has a more favorable stabilization effect relative to Ca-N-X competing phases.

Automation of this analysis is well within reach given the progress described above. Further, the methodologies used to declutter epitaxy analysis and generate heterostructures represent much-needed utilities for the PyMatGen library, and they will therefore be incorporated into the library upon publication. With the oxidation-preventive steps taken experimentally and the stabilization effects predicted computationally, numerous EHMS can be realized.

3. Prediction of Halide-Mobile Materials

Here, we outline a data-mining approach to identify materials with low halide diffusion barriers, where this the first step in discovery of EHAP's for halide-ion batteries. Whereas a screening of EHMS's has not been reported, numerous searches for electride materials have been described. Initial studies by Hosono *et al.* were largely successful in identification of 2-D electrides.[18-19] A series of eight compounds (three M_2N and five M_2C; M=metal) were identified and later experimentally confirmed as electrides.[4] Following these screenings from 2014, searches with substitutional[20] and artificial design[21] search algorithms were described, but with little to no influence on the field due to nearly all identified structures being unstable relative to known phases. Other studies have reported on over 200 combined "electrides" with use of broader electride definitions – i.e. the anionic electron can be largely associated with an atomic orbital and not be truly isolated/anionic.[22-24] These liberal descriptors cause nearly all of the materials to be ignored by experimentalists; however, we adopt their broader definitions for the sake of EHMS's towards halide-ion batteries, rather than a strictly electride-motivated search. Therefore, the term EHMS carries a loose definition herein, where the "electride" may have variable anionic electron character. Reported electrides will be investigated via a DFT analysis, should they have a halogenated analog. Further, this process has been automated for a general search through known halides – that is the reverse search using an EHMS perspective, where halides are the starting point instead of electrides.

3.a. Investigating Known Electride-Halide Systems

To establish known EHMS's, we look at reported electride materials and search for their halide analog pair(s). Metal halide electrides (M_aX_b, X=F,Cl,Br,I) were removed from this analysis in addition to all 0-D electrides. This limits our search to materials that have a 1,2,3-D diffusion pathway along which the halide can percolate. Of the remaining 118 electride materials, each was vetted by searching the Materials Project Database for an isostructural halide. Surprisingly, only 12 electrides were found to have at least one EHAP, where a total of 24 EHAP's were identified. All experimentally known 2-D electrides (under Hosono's strict electride definitions) were found to possess an EHAP – that is M_2N (M= Ca, Sr, Ba) and M_2C (M = Y, Gd, Tb, Dy, Ho) compounds. These R-3m symmetrized electrides made up 8 of the 12 systems and 17 of the 24 EHAP's. Another subgroup encompasses the 1-D electrides under the $P6_3/mcm$ symmetry, namely La_5M_3 (M = Bi, Sb, Pb) compounds. The remaining electride with an EHAP is that of Cs_3O, which also possesses $P6_3/mcm$ symmetry but with a different structure motif. Together, these 12 electrides and their corresponding EHAP's represent the only known EHMS's (examples of these structure types are in Figure 2).

While these EHMS's are known to exist, the fluidity of the analog pairs is not known – that is, whether the electride can be converted to the halide analog(s) and vice-versa. The ability to electrochemically (de)intercalate ions is central to battery applications, so the halide-diffusion barrier must be investigated. The first scrutiny can be made by evaluating vacancy-based diffusion of the halide analogs.

A novel vacancy-based diffusion algorithm is formulated using the PyMatGen and Custodian[7] codes. Given only the halide structure and diffusing species, all symmetrically unique diffusion pathways are identified under a single parameter criterion – the diffusion pathway must be under 6.5 Å in length. Then for each given pathway, a linear-interpolated diffusion calculation is generated. Further, image dependent pair potential (IDPP) relaxation is performed to approximate a nudged-elastic-band (NEB) minimized diffusion pathway.[25] This non-DFT approximation produces a lower energy pathway by minimizing changes in atomic distances along the path, and thus is represents an efficient alternative to a full NEB analysis. Together, the linear interpolation and IDPP diffusion calculations provide a representative characterization of halide diffusion in the structure. This algorithm was applied to the 24 halide analogs in order to given insight on the halide mobility; however, the halides possessed extremely high diffusion barriers (>1eV) in all cases analyzed thus far.

It is also worth noting that 11 of the 12 EHMS's are incomplete, but they can easily be extended by halide substitution of known halide analog(s). For example, the Y_2C system only possesses the Y_2CI_2 analog, whereas no known crystal structure is reported for the Y_2CX_2 (X = F, Cl, Br) compositions. By substitution of other halides into the iodide analog, we

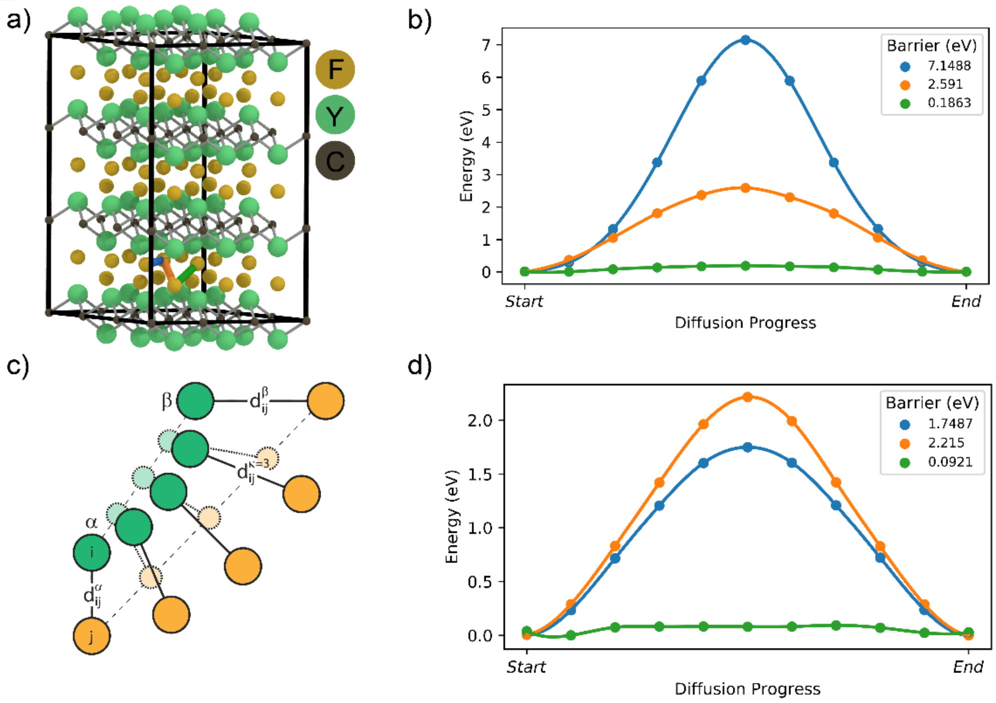

Figure 6. (a) the 3x3x3 superlattice of Y_2CF_2 used for vacancy-based diffusion calculations, where the three unique diffusion pathways for fluoride ions are also shown via the bright orange, green, and blue connections near the bottom of the supercell. The pathway colors correspond to respectively colored curves in plots (b) and (d). **(b)** the linear interpolated diffusion of Y_2CF_2 for each pathway shown in (a). Only the third path (green) shows a low diffusion barrier of 186.3 meV. The remaining pathways show extremely high barriers that agree with long diffusion length (orange) and high ionic radii overlap (blue), as discussed in Section 3b of the main text. **(c)** an illustration of a path generated by linear interpolation (transparent path) versus that of IDPP analysis (opaque path) with start (α) and end (β) coordinates. Image is adapted from reference 25. **(d)** the IDPP diffusion of Y_2CF_2 where we see a 76%, 15%, and 51% decrease in the pathway diffusion barriers and minimum diffusion barrier of 92.1 meV.

can complete the EHMS. Exchange of fluorine for iodine was carried out for the Y_2CX_2 system and shown to have a drastically lower diffusion barrier, relative to all other materials above (Figure 6). This highlights the potential fluidity of this EHAP towards fluoride-ion batteries, and thus, experimental examination is now underway.

In conclusion, investigating known EHMS's is an efficient means towards proposing materials for halide-ion batteries. However, such an approach is largely limited by the number of known systems (12 in total), so while moderately successful, an improved strategy is needed.

3.b. Dehalogenation Analysis of All Halide Systems

The necessity for discovery of EHMS's has been established via the shortcomings of Section 3a – specifically the low number of known EHMS from a database screening. Rather than focus on known electrides as a starting point, the reciprocal approach is taken here: a search of known halide materials toward EHMS's. A halide starting point corresponds to a kinetically trapped system experimentally, so the electride-analog need not be the thermodynamically favored phase (nor be reported previously). Using the vacancy-based diffusion algorithm developed above, all known halide materials can be vetted for halide mobility as a first criterion. Preferential characteristics such as theoretical gravimetric and volumetric capacities then become a secondary analysis. The decision to use characteristics such as capacity as secondary criteria is twofold: first, demonstration of any material for novel halide-ion batteries serves a proof-of-concept step, prior to demonstration of the highest performing system; second, halide-mobility may be desirable in non-battery applications (such as solid electrolytes or membranes), so we extend implications of this screening without including restrictive conditions aimed toward battery applications.

Therefore, we examine all 7,025 halides crystal structures in the Materials Project Database that have the diffusing halide of interest below 50% atomic content. Oxidation state analysis is then performed on each compound using a bond-valence estimation algorithm outlined by O'Keefe and Brese.[26] Using this analysis, we further limit our pool to compounds possessing an electropositive element(s) as well as the diffusing halide in the (-1) oxidation state – narrowing our search to 4,869 structures.

The previously established vacancy-based diffusion algorithm is used to characterize the remaining compounds. Analysis of known EHMS's in the previous section suggest two additional criteria for ranking of crystal structures: diffusion path length and relative 'blocking' of a pathway by a non-participating atom. We limit the diffusion pathway to 5 Å in length, and the ionic radii overlap (see Figure 7 for definition) to 1 Å. These are extremely liberal conditions for diffusion as 3,854 structures remain under these criteria. This issue is negated because we rank the structures under identical criteria. That is, the applied algorithm records all diffusion lengths and ionic radii overlap for each structure pathway, and the structures with lowest length/overlap pathways are analyzed first. This strategic ranking will allow us to isolate the structures with highest halide-mobility first as well as determine the relationship between these criteria and diffusion energy barrier. Should other criteria be more important in halide mobility (e.g. symmetry or element types), these can be later isolated. Together, we expect to pull out halide-mobile materials in addition to formulating general laws that govern mobility across all structure types.

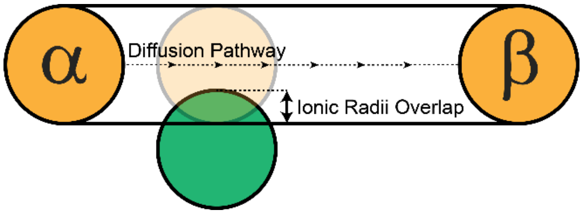

Figure 7. Illustration of ionic radii overlap that is referred to in the main text. The overlap is defined as the maximum overlap of the diffusing ion with another atom as it moves along from the start (α) to end (β) of the diffusing pathway. This illustrates the overlap in 2D space for simplification, but the same definition applies in 3D space with ionic spheres.

3.c. Future Work

At the current stage, a substantial number of diffusion calculations need to be completed, where the code performs this work and minimal human intervention is required. Thus, efforts can be focused towards follow-up studies on these materials.

The first follow-up study should be the relative stability of the fully deintercalated material (the "electride" analog). This should be done alongside halide single-atom diffusion analysis through the electride material. Further, automated analysis of secondary properties for battery applications can easily be carried out (e.g. theoretical values for gravimetric capacities, volumetric capacities, voltages, and work functions). The code related to these analyses will be established while the vacancy-based diffusion calculations are underway, allowing for a quick follow-up study of halide-mobile materials.

4. Concluding Remarks

In summary, we have established a robust framework for EHMS discovery and synthesis which was heavily benchmarked against known systems. Initially limited to 12 systems, we seek to experimentally demonstrate EHAP fluidity with electrochemical cycling. However, validation with known EHMS's is extremely challenging due to the systems' oxidizing nature and high halide diffusion barriers. Intensive oxidation-deterring procedures were established, and a means thin-film stabilization is outlined computationally to synthesize such materials. Further, ideal systems are identified from both perspectives of an EHMS (i.e. from known electrides and from known halides). Halide diffusion analysis will help isolate halide-mobile systems to be synthesized via a substrate-stabilization strategy and then tested towards a halide-ion battery application.

5. Calculation Details

All slab calculations are carried out according to the Materials Virtual Lab standards (MVLSlabSet) while using the VASP code. This entails a PBE functional along with a 400 eV cutoff and AxBxC Monkhorst–Pack grid ($A=50/a$ and $B=50/b$, where a and b are lattice vectors. $C=1$ for slabs and $C=50/c$ for bulk). All energies were converged to 0.1 meV under Gaussian smearing.

The series of 10 slabs and their corresponding σ energies and thicknesses (h) are fit to the exponential decay equation: $\sigma = AB^h + E_S$, where A and B are arbitrary constants. The SciPy package is used to fit this equation. Starting guesses $A=1$, $B=0.95$, and $E_S=max(\sigma)$ drastically improved the quality of fits.

All diffusion calculations are carried out according to the Materials Project standards (MPStaticSet) while using the VASP code. This entails a PBE functional along with a 520 eV cutoff and AxBxC Monkhorst–Pack grid ($A=100/a$; $B=100/b$; $C=100/c$; where a, b, and c are lattice vectors). All energies were converged to 0.5 meV under tetrahedron-method smearing with Blöchl corrections.

6. Acknowledgements

Thank you to Jon Meyer for aiding in the vacuum system design. He allowed me to examine the Cahoon Lab's system, and further, he explained the fundamentals of such a build. Jon and I are now working towards a co-authored paper on CVD basics, and he has made possible the development of an educational-based computer application.

Jacob Pawlik assisted in the benchmark synthesis of Sr_2N, where we ran many of these experiments together. I would also like to accredit him for acquisition of the XRD diffractogram shown in Figure 3. In addition to Jacob, Daniel Druffel and Adam Woomer were heavily influential in the planning of experiments – through open discussions as well as subgroup meetings.

I would also like to thank a number of specialists in the setup of VASP, PhonoPy, USPEX, CALYPSO, and PyMatGen capabilities for our lab. Michael Waldron, Shubin Liu, and Jenny Williams aided in the installation and troubleshooting of these packages onto the UNC computing clusters. Likewise, thank you to Matt Horton (UC Berkley) and Shyue Ping Ong (UC San Diego) who aided in bug-fixing PyMatGen issues where I encountered them.

Lastly and most importantly, thank you to Scott Warren and the Warren Lab for aiding in the formulation of this project and the intellectual merits stemming from it.

7. Supporting References

1. K. Lee, S. W. Kim, Y. Toda, S. Matsuishi and H. Hosono, *Nature*, **2013**, 494, 336–340.
2. M. Kitano, Y. Inoue, H. Ishikawa, K. Yamagata, T. Nakao, T. Tada, S. Matsuishi, T. Yokoyama, M. Hara and H. Hosono, *Chem. Sci*., **2016**, 7, 4036–4043.
3. S. Kim, S. Song, J. Park, H. S. Yu, S. Cho, D. Kim, J. Baik, D. H. Choe, K. J. Chang, Y. H. Lee, S. W. Kim and H. Yang, *Nano Lett*., **2017**, 17, 3363–3368.
4. D. L. Druffel, A. H. Woomer, K. L. Kuntz, J. T. Pawlik, S. C. Warren, *J. Mater. Chem. C*, 2017, 5, 11196-11213.
5. Y. Prots, G. Auffermann, M. Tovar and R. Kniep, *Angew. Chem., Int. Ed*., **2002**, 41, 2288–2290.
6. M. Hellenbrandt*, Crystallogr. ReV*. 2004, 10, 17-22.
7. S. P. Ong, W. D. Richards, A. Jain, G. Hautier, M. Kocher, S. Cholia, D. Gunter, V. Chevrier, K. A. Persson, G. Ceder, *Comp. Mat. Sci*., **2013**, 68, 314–319.
8. H. Ding, S. S. Dwaraknath, L. Garten, P. Ndione, D. Ginley, and K. A. Persson, *ACS Appl. Mater. Interfaces*, **2016**, 8 (20), 13086–13093.
9. A. Zur and T. C. McGill, *J. of Appl. Phys*., 1984 55, 378
10. M. de Jong, W. Chen, T. Angsten, A. Jain, R. Notestine, A. Gamst, M. Sluiter, C. K. Ande, S. van der Zwaag, J. J. Plata, C. Toher, S. Curtarolo, G. Ceder, K. A. Persson, M. Asta, *Scientific Data*, **2015**, 2, 150009.
11. A. Jain, S.P. Ong, G. Hautier, W. Chen, W.D. Richards, S. Dacek, S. Cholia, D. Gunter, D. Skinner, G. Ceder, K.A. Persson, *APL Materials*, **2013**, 1(1), 011002.
12. T.B. Reed, Free Energy of Formation of Binary Compounds: An Atlas of Charts for High-Temperature Chemical Calculations. *Cambridge, Mass: MIT Press*, **1971**. Print.
13. A. Jain, G. Hautier, S. P. Ong, C. Moore, C. Fischer, K. Persson, G. Ceder, *Physical Review B*, **2011**, 84(4), 045115.
14. https://www.mtixtl.com/crystalssubstratesa-z.aspx
15. A. H. Woomer, D. L. Druffel, J.D. Sundberg, J. T. Pawlik, S.C. Warren, *under review*
16. A. K, Lenstra, H. W. Lenstra Jr., L. Lovász, *Mathematische Annalen*, **1982**, 261(4), 515–534.
17. S. Zhu, F.Peng, H. Liu, A. Majumdar, T. Gao., Y. Yao, *Inorg. Chem*. **2016**, 55 (15), 7550-7555.
18. T. Tada, S. Takemoto, S. Matsuishi, H. Hosono, *Inorg. Chem*. **2014**, 53(19), 10347-10358.
19. T. Inoshita, S. Jeong, N. Hamada, H.Hosono, *Phys. Rev. X*, **2014**, 4, 031023.
20. W. Ming, M. Yoon, M. H. Du, K. Lee, S. W. Kim, *J. Am. Chem. Soc*. **2016**, 138, 15336−15344.
21. Y. Zhang, H. Wang, Y. Wang, L. Zhang, Y. Ma, *Phys. Rev. X*, **2017**, 7, 011017.
22. L. A. Burton, F. Ricci, W. Chen, G. Rignanese, G. Hautier, *Chem. Mater*. **2018**, 30, 7521−7526.
23. J. Zhou, L. Shen, M. Yang, H. Cheng, W. Kong, Y. P. Feng, *Chem. Mater*. **2019**, 31, 1860−1868.
24. Q. Zhu and T. Frolov, arXiv:1812.06222.
25. S. Smidstrup, A. Pedersen, K. Stokbro, H. Jónsson, *J. Chem. Phys*., **2014**, 140, 214106.
26. M. O’Keeffe and N. E. Brese, *J. Am. Chem. Soc*. **1991**, 113, 3226-3229.